Fermi Surface Nesting in Disordered $Cu_{1-x}Pd_x$ Alloys

I. Wilkinson, R. J. Hughes, Zs. Major, S. B. Dugdale, and M. A. Alam
H. H. Wills Physics Laboratory, University of Bristol, Tyndall Avenue, Bristol, BS8 1TL, United Kingdom

E. Bruno, B. Ginatempo, and E. S. Giuliano
Dipartimento di Fisica and Unità INFM, Università di Messina Salita Sperone 31, 98166 Messina, Italy
(Received 26 March 2001; published 31 October 2001)

The concentration-dependent position of the diffuse peaks in electron and x-ray diffraction patterns of $Cu_{1-x}Pd_x$ alloys in the disordered state is attributed to Fermi surface nesting. We present the first experimentally determined Fermi surfaces of $Cu_{0.72}Pd_{0.28}$ and $Cu_{0.6}Pd_{0.4}$, and show that they do indeed possess significant flat areas capable of nesting. Moreover, the magnitudes of the nesting vectors are in excellent agreement with those deduced from electronic structure calculations and diffraction experiments.

DOI: 10.1103/PhysRevLett.87.216401 PACS numbers: 71.18.+y, 74.70.Ad, 78.70.Bj, 81.30.Hd

The shape of the Fermi surface (FS) often results in a variety of ordering phenomena in metals. These arise because of large areas of parallel or near-parallel sheets of FS which can "nest" with each other, resulting in a significant enhancement of those electronic excitations with a wave vector $\mathbf{q}$ which spans the parallel sections. Spin- and charge-density waves [1] are two examples of FS-driven orderings, where the periodicity of the modulation of the conduction electrons is determined by a nesting vector on the FS.

The study of the short-range compositional order found in many binary metallic alloys above the order-disorder transition temperature (T_c) provides valuable insight into the phase behavior of these systems [2,3]. The origin of the short-range order (SRO) often lies in a nestable FS, in a manner analogous to the way nesting may yield a paramagnetic state susceptible to magnetic order. Indeed, it was just this idea that led Moss to suggest that measurements of the diffuse scattering in x-ray and electron diffraction patterns could be used to make inferences about the FS topology of disordered alloys [4].

One system that has been extensively studied is $Cu_{1-x}Pd_x$ (see [5] for phase diagram), where the nesting is thought to be particularly strong. Below T_c ($\sim$800 K), this system adopts either the B2 or $L1_2$ long-range ordered structure or one of a wealth of long period superstructures, depending on composition (see, for example, [6,7]). The SRO is found over a temperature range of a few hundred degrees above T_c, and is experimentally observed as a splitting of the $\langle 100 \rangle$ and $\langle 110 \rangle$ diffuse scattering peaks for alloys with a composition between 13–60 at. % Pd [8,9]. The separation of the peaks is very sensitive to the alloy concentration [8,10], and there is an excellent correlation between the periodicity of the SRO as measured by the peak separation and the FS nesting vectors predicted by first-principles band-theoretic calculations [11]. Furthermore, it has been suggested that incommensurability between the nesting vector and parent lattice may be a factor in the formation of the low-temperature ordered phases [5]. These studies provide strong evidence that the FS plays a crucial role in determining the ordering behavior of $Cu_{1-x}Pd_x$, but direct measurements of its FS topology and nesting features have never been performed. In this Letter we present the first three-dimensional FS of $Cu_{0.72}Pd_{0.28}$ and $Cu_{0.6}Pd_{0.4}$ together with quantitative assessments of their nesting tendencies, and supporting band theoretical calculations.

One of the first microscopic theories explaining the occurrence of SRO is that of Krivoglaz, Clapp, and Moss (KCM) [12,13], and describes the diffuse intensity in terms of a short-range order parameter, $\alpha(\mathbf{q})$. This is itself a function of $v(\mathbf{q})$, the Fourier transform of the pairwise interaction potential combination, $v(\mathbf{r}) = v^{AA}(\mathbf{r}) + v^{BB}(\mathbf{r}) - 2v^{AB}(\mathbf{r})$. Minima in $v(\mathbf{q})$ cause maxima in $\alpha(\mathbf{q})$ and an intensity peak in the diffraction pattern. Assuming the FS to be sufficiently well defined in a random alloy, the argument proceeds by asserting that the conduction electrons' contribution to $v(\mathbf{q})$ is significant. Minima of $v(\mathbf{q})$ then occur at nesting wave vectors, and the "strength" of the nesting (the extent of the flat areas) relates to the intensity of the diffuse peaks. In addition, the size of the nesting vector determines the peak separation. Furthermore, along $\langle 110 \rangle$ the FS of Cu is convex, while the Γ-centered FS sheet of Pd is concave—it is easy to imagine some intermediate composition with a FS that has significant flat areas perpendicular to $\langle 110 \rangle$. The movement of the peaks with Pd concentration may also be qualitatively understood, as the Fermi wave vector along $\langle 110 \rangle$ must reflect the change in electron per atom ratio and hence the occupied fraction of the Brillouin zone (BZ).

A significant advance in the understanding of such systems came with the *ab initio* electronic description of compositional order, pioneered by Gyorffy *et al.* [14]. Band structure calculations were performed via the self-consistent Korringa-Kohn-Rostoker (KKR) technique, within the coherent potential approximation (CPA) to describe the substitutional disorder, and the local-density approximation for the exchange-correlation potential.

Here the SRO is described not by $v(\mathbf{q})$, but by the mean-field approximation to the direct correlation function, $S^{(2)}(\mathbf{q})$. The SRO parameter, $\alpha(\mathbf{q})$, is then given by

$$\alpha(\mathbf{q}) = \frac{\beta x(1-x)}{1-\beta x(1-x)S^{(2)}(\mathbf{q})}, \quad (1)$$

where $\beta = 1/(k_B T)$ and x the concentration of one of the species. The important distinction from the KCM theory is that it is the *peaks* in the direct correlation function that determine the most stable ordering modulation. In a mean-field theory afforded by the CPA [14], $S^{(2)}(\mathbf{q})$ has the form

$$S^{(2)}(\mathbf{q}) \propto \sum_{\mathbf{k}} \iint \frac{f(\varepsilon_{\mathbf{k}}) - f(\varepsilon'_{\mathbf{k}+\mathbf{q}})}{\varepsilon_{\mathbf{k}} - \varepsilon'_{\mathbf{k}+\mathbf{q}}} \times A(\mathbf{k},\varepsilon)A(\mathbf{k}+\mathbf{q},\varepsilon')\, d\varepsilon\, d\varepsilon', \quad (2)$$

where $f(\varepsilon_{\mathbf{k}})$ is the usual Fermi occupation function, and $A(\mathbf{k},\varepsilon)$ the compositionally averaged Bloch spectral function (which may be thought of as a density of states per $\mathbf{k}$ point). If $\mathbf{q}$ is a nesting vector on the FS, the denominator in Eq. (2) is vanishingly small and its contribution to $S^{(2)}(\mathbf{q})$ considerable.

The only remaining question is one of FS definition; the proposed mechanism requires a FS with a low level of disorder scattering to preserve the nesting. The peak width of the Bloch spectral function at the Fermi energy may be interpreted as an inverse lifetime of electrons at the Fermi level, and thus a measure of the "sharpness" of the FS. Gyorffy *et al.* [14] found a relatively well-defined FS on the scale of its dimensions. Similarly, the order parameter $\alpha(\mathbf{q})$ derived from $S^{(2)}(\mathbf{q})$ contains the split peaks as expected, and their movement with concentration is in good agreement with experiment [11]. The calculated FS shows progressive flattening along $\langle 110 \rangle$ with increasing Pd concentration, and it was flattest for a composition of around 40 at. % Pd [11].

The two dimensional angular correlation of electron-positron annihilation radiation (2D-ACAR) technique is capable of providing the topological information required to assess the nesting capabilities of the $Cu_{1-x}Pd_x$ FS, and is of particular utility here as more conventional quantum-oscillatory methods are often precluded by the disorder scattering inherent in a random alloy. Previous 2D-ACAR studies of the $Cu_{1-x}Pd_x$ system [15] showed a trend towards flattening with increased Pd concentration but, yielding only linear projections of the FS, could not provide any information about its nesting properties.

In a 2D-ACAR measurement, the occupied momentum states, and hence the FS, are accessed via a once-integrated projection of the underlying two-photon momentum density $\rho(\mathbf{p}) = \sum_{j,\mathbf{k},\mathbf{G}} n^j(\mathbf{k}) |C_{\mathbf{G},j}(\mathbf{k})|^2 \delta(\mathbf{p}-\mathbf{k}-\mathbf{G})$. $n^j(\mathbf{k})$ is the $\mathbf{k}$-space electron occupation density of the jth band, $C_{\mathbf{G},j}(\mathbf{k})$ are the Fourier coefficients of the interacting electron-positron wave-function product, and the delta function expresses the conservation of crystal momentum. The change in occupancy as a band crosses the Fermi level, E_F, results in discontinuities in $\rho(\mathbf{p})$ not only at the Fermi wave vector $\mathbf{k}_F$, but also at $\mathbf{k}_F + \mathbf{G}$, where $\mathbf{G}$ is a reciprocal lattice vector. It is possible to reconstruct the full 3D momentum density from a small number of projections along different crystallographic directions [16–18], a strategy which has already successfully revealed the nested FS of other systems [19]. If the positron wave function is sufficiently slowly varying, and may almost be considered independent of $\mathbf{k}$, the Lock-Crisp-West (LCW) prescription [20] can be applied. In this procedure, the higher momentum components are folded back into the first BZ, superimposing the discontinuities in $\rho(\mathbf{p})$, and giving the occupancy in $\mathbf{k}$ space.

To complement our experimental data with quantitative theoretical predictions, fully relativistic self-consistent electronic structure calculations were made of the measured compositions. As in the calculations of Gyorffy *et al.* [14], the KKR-CPA method was used [21]. Fully relativistic calculations were considered necessary as Pd is a sufficiently heavy element for spin-orbit effects to be important [22]. From the self-consistent potentials, the FS was identified from peaks in the Bloch spectral function evaluated at the Fermi energy. The $\mathbf{k}$-space smearing due to disorder was of the order of 1% of the BZ size, much smaller than the experimental resolution, and not large enough to destroy any nesting propensities (or to allow different levels of disorder to be distinguished in the momentum densities).

The 40 at. % Pd sample was chosen as this represents the alloy expected to have the strongest nesting, and a further measurement at 28 at. % Pd allows the evolution of the FS with concentration to be monitored. Both samples were single crystals grown using the Bridgeman technique in an argon atmosphere, and are effectively quenched in the disordered phase; ordering requires several weeks of annealing just below T_c. That the crystals were in the fcc phase was confirmed through Laue back-reflection prior to measurement. A total of five spectra were measured for each sample, along directions regularly spaced between Γ-X and Γ-K. More than 400×10^6 (effective) counts were collected in each spectrum, at a sample temperature of $\sim$50 K. The resolution of the Bristol spectrometer at this temperature is approximately 4% of the BZ dimension. A maximum entropy based deconvolution routine [23] was employed to suppress the smearing effect of finite instrument resolution prior to reconstruction of the 3D $\rho(\mathbf{p})$. Application of the LCW prescription yielded the electron occupation in $\mathbf{k}$ space. In performing the LCW procedure (and band structure calculations), the lattice parameters of the alloys were linearly interpolated between those of pure Cu (3.61 Å) and pure Pd (3.89 Å). The relaxed lattice constants obtained from our KKR-CPA calculations differed from Vegard's rule by less than 1%; such a difference

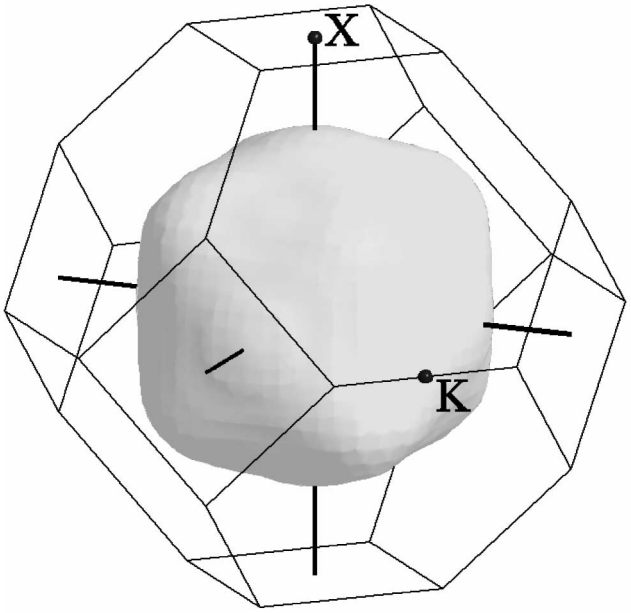

FIG. 1. The Fermi surface of $Cu_{0.6}Pd_{0.4}$, reconstructed from 2D-ACAR projections.

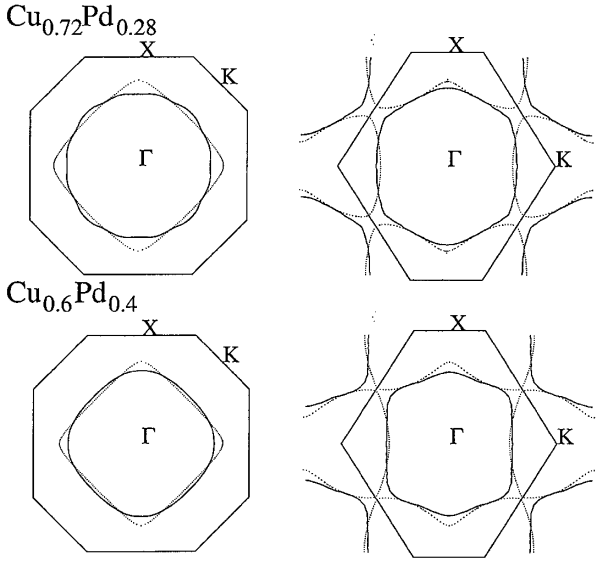

FIG. 2. (100) (left hand side) and (110) (right hand side) planes through the Fermi surface of $Cu_{0.72}Pd_{0.28}$ (top) and $Cu_{0.6}Pd_{0.4}$ (bottom). The solid lines represent the experimental data and the dashed lines the KKR-CPA calculation; the boundary and selected symmetry points of the first BZ are also shown. The magnitudes of FS extremal vectors parallel to Γ-X and Γ-K are presented in Figs. 3 and 4.

in lattice constant was found to modify the experimentally derived nesting vectors by less than 0.5%. Figure 1 shows the reconstructed FS of $Cu_{0.6}Pd_{0.4}$. It consists of a closed Γ-centered sheet, with distortions along Γ-L that would, at higher Cu concentrations, enlarge to form the familiar necks in the FS of pure Cu.

Figure 2 shows the FS in the (100) and (110) planes through the Γ point for the two compositions along with appropriate slices from the KKR-CPA calculations. Considering first the (100) plane, the measured FS sections do indeed show flattened edges perpendicular to Γ-K, and as expected, the $Cu_{0.72}Pd_{0.28}$ plane is distinctly less flat than its counterpart. Both are in good agreement with calculation. That the flat sections also extend along [100] out of the (100) plane is evident from the FS in the (110) plane, plotted on the right hand side of Fig. 2; at 40 at. % Pd, they remain flat across half the height of the BZ. It is also interesting to note that the calculations predict the system to be near an electronic topological transition where the necks would close at 40 at. % Pd, whereas the experiment is showing that the FS is already simply connected at 28 at. % Pd. This is most likely a consequence of the approximations used in the calculations, namely the local density description of exchange-correlation or the mean-field nature of the coherent potential approximation.

In an effort to assess the extent of the nestable area, a histogram of FS spanning vectors in the ⟨110⟩ and (for comparison) ⟨100⟩ directions was compiled. These vectors lie in planes perpendicular to Γ-X, and in the top halves of Figs. 3 and 4 these histograms are plotted, as a function of distance from the Γ point along Γ-X, in the form of a density map; the darkest areas represent the peaks in the histogram. From these figures it is possible to observe how the nesting vectors along the two directions [in the (001) plane] evolve as a function of distance along Γ-X. It is clear that in the ⟨110⟩ direction, the histogram peak occurs at the same position for much of the BZ, while it steadily decreases for the ⟨100⟩ direction. Summation over all planes yields a histogram of spanning vectors for the whole BZ, and these are shown in the bottom halves of Figs. 3 and 4. The existence of strong nesting along ⟨110⟩ is evident from the sharp peak in the ⟨110⟩ histogram for $Cu_{0.6}Pd_{0.4}$. Integrating under the peak gives an indication

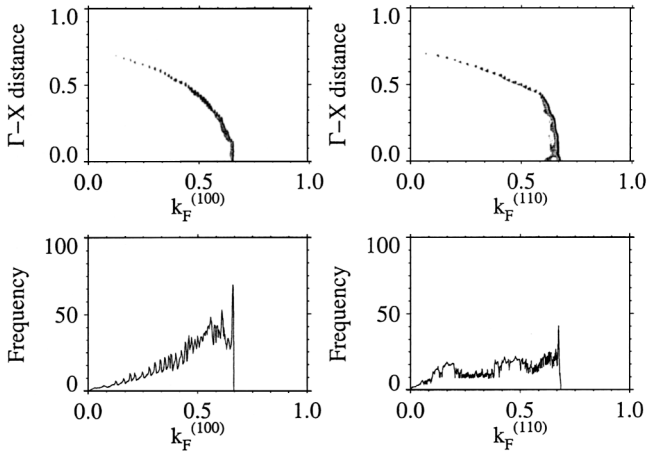

FIG. 3. $Cu_{0.72}Pd_{0.28}$: Plane by plane histogram of spanning vectors, as fractions of $(\frac{2\pi}{a})$, in the ⟨100⟩ (top left) and ⟨110⟩ (top right) directions. The total histograms (summed over all planes) for the same directions are shown below their planar decompositions.

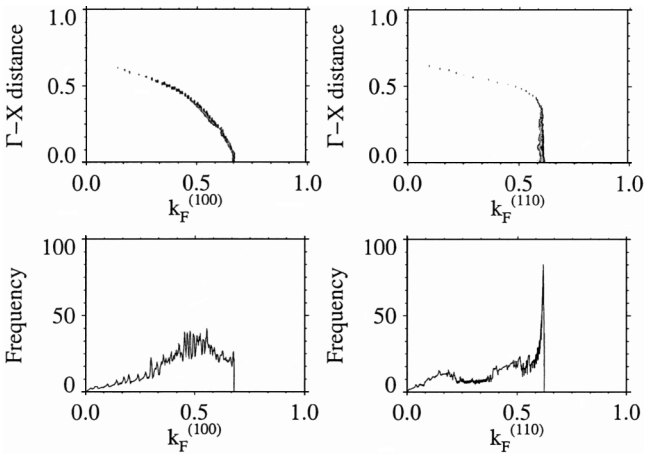

FIG. 4. $Cu_{0.6}Pd_{0.4}$: As Fig. 3. Strong nesting along ⟨110⟩ is clearly evident.

of the fraction of the FS which participates in the nesting. For $Cu_{0.72}Pd_{0.28}$, we find that 10 ± 1% of the FS area is nestable, but for $Cu_{0.6}Pd_{0.4}$ this has risen to 23 ± 1%, in agreement with the observation of more intense diffuse scattering peaks from the latter.

The histogram analysis also yields a precise caliper of the nesting vectors of our reconstructed FS, and these are collected in Table I. Also presented are magnitudes of the Fermi wave vector in the ⟨110⟩ direction, $\mathbf{k}_F^{(110)}$, both calculated [11] and determined experimentally [8]. While our calculated FS dimensions are in excellent agreement with the work of others, experiment consistently finds a greater $\mathbf{k}_F^{(110)}$. This may be seen in Fig. 2, where the calculated FS appears inside its experimental counterpart along the ⟨110⟩ direction.

In conclusion, it is believed that FS nesting drives the SRO found in $Cu_{1-x}Pd_x$ alloys above T_c; the FS is responsible for determining which constituent atom will occupy a particular lattice site. Support for this idea is provided by band structure calculations, which predict a relatively well-defined FS with significant flat areas perpendicular to ⟨110⟩. The strongest nesting occurs at around 40 at.% Pd, and the evolution of the calculated nesting vector agrees well with the movement of the diffuse scattering peaks with varying composition. We have measured the FS topologies of two representative members of the $Cu_{1-x}Pd_x$ series, and shown that both have strong nesting in the ⟨110⟩ direction, the $Cu_{0.6}Pd_{0.4}$ composition in particular. The magnitudes of the nesting vectors obtained are in excellent accord with both the predictions of calculations and diffraction experiments. These observations provide the vindication of the FS mechanism proposed more than three decades ago.

TABLE I. Values of $\mathbf{k}_F^{(110)}$ as a fraction of $(\frac{2\pi}{a})$, measured from our experiment and calculations. Also shown are corresponding values measured by Oshima and Watanabe (taken from Fig. 10 of [8]), and those calculated by Gyorffy *et al.* (taken from Fig. 2 of [11]).

At. % Pd	Current expt.	Oshima and Watanabe[a]	Current calculations	Gyorffy *et al.*[a]
28	0.66 ± 0.01	0.65 ± 0.01	0.63 ± 0.01	0.64 ± 0.01
40	0.61 ± 0.01	0.60 ± 0.01	0.60 ± 0.01	0.60 ± 0.01

[a]Quoted errors reflect the accuracy with which values could be taken from the cited figures, not the precision of the original work.

The authors thank the EPSRC (U.K.) and the Instituto Nazionale di Fisica della Materia (PAIS ELMAMES) (Italy) for financial support, and B. Gyorffy for useful discussions. One of us (S. B. D.) acknowledges generous support from the Royal Society.

[1] E. Fawcett, Rev. Mod. Phys. **60**, 209–283 (1988); A. G. Khachaturyan, *Theory of Structural Transformations in Solids* (Wiley, New York, 1983).
[2] H. Sato and R. S. Toth, in *Alloying Behaviour and Effects in Concentrated Solid Solutions,* edited by B. T. Massalski (Gordon and Breach, New York, 1965).
[3] M. A. Krivoglaz, *Diffuse Scattering of X-Rays and Neutrons by Fluctuations* (Springer, Berlin, 1996).
[4] S. C. Moss, Phys. Rev. Lett. **22**, 1108 (1969).
[5] E. Bruno, B. Ginatempo, and E. S. Giuliano, Phys. Rev. B **63**, 174107 (2001).
[6] D. Broddin *et al.,* Philos. Mag. A **54**, 395 (1986).
[7] G. Ceder *et al.,* Acta Metall. Mater. **38**, 2299 (1990).
[8] K. Oshima and D. Watanabe, Acta Crystallogr. Sect. A **29**, 520 (1973).
[9] K. Oshima, D. Watanabe, and J. Harada, Acta Crystallogr. Sect. A **32**, 883 (1976).
[10] M. Rodewald *et al.,* Phys. Rev. B **55**, 14 173 (1997).
[11] B. L. Gyorffy and G. M. Stocks, Phys. Rev. Lett. **50**, 374 (1983).
[12] M. A. Krivoglaz, *Theory of X-ray and Thermal Neutron Scattering by Real Crystals* (Plenum Press Inc., New York, 1969).
[13] P. C. Clapp and S. C. Moss, Phys. Rev. **142**, 418 (1966); **171**, 754 (1968).
[14] B. L. Gyorffy *et al.,* in *Alloy Phase Stability,* edited by G. M. Stocks and A. Gonis (Kluwer Academic Publishers, Dordrecht, 1989).
[15] L. C. Smedskjaer *et al.,* Phys. Rev. Lett. **59**, 2479 (1987).
[16] A. M. Cormack, J. Appl. Phys. **34**, 2722 (1963).
[17] A. M. Cormack, J. Appl. Phys. **35**, 2908 (1964).
[18] G. Kontrym-Sznajd, Phys. Status Solidi A **117**, 227 (1990).
[19] S. B. Dugdale *et al.,* Phys. Rev. Lett. **79**, 941 (1997); H. M. Fretwell *et al.,* Phys. Rev. Lett. **82**, 3867 (1999).
[20] D. G. Lock, V. H. C. Crisp, and R. N. West, J. Phys. F **3**, 561 (1973).
[21] E. Bruno and B. Ginatempo, Phys. Rev. B **55**, 12 946 (1997).
[22] E. Bruno, B. Ginatempo, and E. S. Giuliano, Phys. Rev. B **52**, 14 557 (1995).
[23] S. B. Dugdale *et al.,* J. Phys. Condens. Matter **6**, L435 (1994); H. M. Fretwell *et al.,* Europhys. Lett. **32**, 771 (1995).